Eur. Phys. J. B **2**, 169–176 (1998)

THE EUROPEAN PHYSICAL JOURNAL B

Transport and thermodynamic properties of $CeAuAl_3$

S. Paschen, E. Felder, and H.R. Ott[a]

Laboratorium für Festkörperphysik, Eidgenössische Technische Hochschule-Hönggerberg, 8093 Zürich, Switzerland

Received: 6 November 1997 / Accepted: 17 November 1997

Abstract. We present measurements of the specific heat, the electrical resistivity, the Hall effect, and the magnetic susceptibility of $CeAuAl_3$, a new heavy–electron compound that crystallizes in an ordered derivative of the tetragonal $BaAl_4$–type structure. For comparison we have also done some of these measurements on the isostructural non–magnetic reference compound $LaAuAl_3$, which appears to be a simple metal. Below $T_N = 1.32$K, $CeAuAl_3$ orders antiferromagnetically and below 1K, we encounter Fermi liquid behaviour with considerably enhanced effective masses, *i.e.*, a quadratic temperature dependence of the resistivity with a large prefactor and a sizable linear–in–T contribution to the specific heat. This linear–in–T contribution increases by more than a factor 50 from its value at $T \gg T_N$ to its value at $T < T_N$. Consequently $CeAuAl_3$ develops a heavy–electron ground state, coexisting with antiferromagnetic order. The small energy scales involved in the problem make $CeAuAl_3$ a good candidate for tuning it, by varying external parameters, towards a quantum critical point. At high temperatures we observe local moment behaviour. From the temperature dependence of the magnetic susceptibility and the specific heat we have derived the crystalline–electric–field–split level scheme of the Ce^{3+} $J = 5/2$ multiplet. Distinct features in the electrical resistivity provide additional evidence for this level splitting.

PACS. 75.20.Hr Local moment in compounds and alloys; Kondo effect, valence fluctuations, heavy fermions – 75.50.Ee Antiferromagnetics – 72.15.-v Electronic conduction in metals and alloys

1 Introduction

Heavy–electron compounds containing Ce have attracted a great deal of attention in the past and are still at the focus of interest today. Considered as particularly intriguing are those compounds in which the Kondo and the Rudermann–Kittel–Kasuya–Yosida (RKKY) interaction are of similar strength. Such a situation may arise if the hybridization width $\Delta \approx \pi \langle V_{sf} \rangle^2 N(E_F)$ (where V_{sf} is the hybridization strength and $N(E_F)$ is the density of states at the Fermi level E_F) is smaller than, but comparable to the position of the 4f level (E_f) relative to the Fermi level $E_0 = |E_f - E_F|$ [1]. Magnetically ordered Kondo lattice systems with reduced moments are expected in this case and have indeed been observed experimentally [2,3].

According to Hulliger [4], both $CeAuAl_3$ and the reference compound $LaAuAl_3$ crystallize in the $BaNiSn_3$–type structure, which is an ordered derivative of the body centered tetragonal $BaAl_4$ structure. For $CeAuAl_3$ Schank *et al.* [5] came to the same conclusion. The room temperature lattice parameters cited in reference [4] are $a = 4.3318(2)$ Å and $c = 10.8390(7)$ Å for $CeAuAl_3$, and $a = 4.3660(3)$ Å and $c = 10.8445(8)$ Å for $LaAuAl_3$. The point group of $CeAuAl_3$ is C_{4v} (or 4 mm) and the symmetry of the Ce site is C_{4v} as well.

[a] e-mail: ott@solid.phys.ethz.ch

To our knowledge the only published data on physical properties of $CeAuAl_3$ are results of resistivity and magnetic susceptibility measurements [5] in the temperature range $T > 2$ K and magnetic susceptibility measurements [4] at $T > 1.6$ K. A variety of observations, including heavy–electron antiferromagnetism, Kondo effect, and crystalline electric field effects, have been made in studies of the series of $CeTMAl_3$ (TM = Pd, Pt, Cu) compounds [5–7]. The related compound $CeAuGa_3$ has been reported [8] to order ferromagnetically below 3.5K. A direct comparison with $CeAuAl_3$ is, however, not straightforward because these other compounds were claimed to crystallize, unlike $CeAuAl_3$, in a disordered variant of the $BaAl_4$ structure. For CeAuAl, which crystallizes in an orthorhombic TiNiSi–type structure, Kondo lattice behaviour and antiferromagnetic ordering have been reported [9,10]. The Ce–Ce distance in $CeAuAl_3$ is with 4.3318(2) Å larger than in $CeCuAl_3$, in $CePtAl_3$, and in CeAuAl [11], and smaller than in $CePdAl_3$ and in $CeAuGa_3$.

2 Samples and experimental details

All the measurements on $CeAuAl_3$ presented in this paper were done using samples cut from the same polycrystalline $CeAuAl_3$ ingot. Likewise, all measurements

on the reference compound $LaAuAl_3$ reported below were done using samples cut from the same polycrystalline $LaAuAl_3$ ingot. Both materials were synthesized following the procedure given in reference [4] by reacting the constituent elements (Ce and La from Research Chemicals, Phoenix, nominally 3N grade; Au from Métaux Précieux, Neuchâtel, nominally grade 4N; Al from Alusuisse, Neuhausen, nominally grade 4N7) in an argon arc furnace, and they were subsequently annealed for one month at 750 °C and at 735 °C, respectively.

The specific heats C_p of $CeAuAl_3$ and $LaAuAl_3$ were measured in the temperature range between 0.044 and 16.2 K and between 1.7 and 20 K, respectively, using a relaxation type method. The electrical resistivities of $CeAuAl_3$ and $LaAuAl_3$ were measured between 0.3 and 300 K and between 1.5 and 300 K, respectively, using a standard four–wire low–frequency ac technique. The Hall effect of $CeAuAl_3$ was measured at several temperatures between 130 and 250 K in magnetic fields up to 70 kOe. A standard setup with the two Hall voltage contacts perpendicular to the current **I** and to the magnetic field **H** was used. In order to eliminate the misalignement voltage, the sample was, at each field value, first measured in an upright position, then turned by 180°, and subsequently measured in a downward position. During a sweep of the magnetic field, the temperature was stabilized with a capacitance thermometer.

The static magnetic susceptibilities χ of $CeAuAl_3$ and $LaAuAl_3$ were measured between 2 and 300 K in an external magnetic field of 500 Oe using a moving sample SQUID magnetometer. Between 0.3 and 2.5 K, we measured the ac susceptibility of $CeAuAl_3$ by a conventional mutual inductance technique with an excitation field of 0.1 Oe and a frequency of 420 Hz. We matched these data to the dc results in the overlapping temperature range between 2 and 2.5 K.

3 Experimental results and discussion

3.1 Specific heat

In Figure 1 we present the specific heat C_p of $CeAuAl_3$ as a function of temperature as full circles. The most prominent feature is a λ–type anomaly with a maximum at $T_N = 1.32$ K. Together with results from our magnetic susceptibility measurements to be outlined below, we identify this anomaly as resulting from the transition to an antiferromagnetically ordered state below the Néel temperature T_N.

In the following we attempt to separate the different contributions to the total specific heat C_p of $CeAuAl_3$. The λ–type anomaly makes a direct evaluation of the lattice contribution unreliable. Therefore we shall use our specific heat measurements of $LaAuAl_3$ to determine this contribution indirectly by assuming that the lattice contributions of $LaAuAl_3$ and $CeAuAl_3$ are the same. This is most probably not too crude an approximation since the two compounds have the same crystal structure and only slightly different ionic masses and cell parameters.

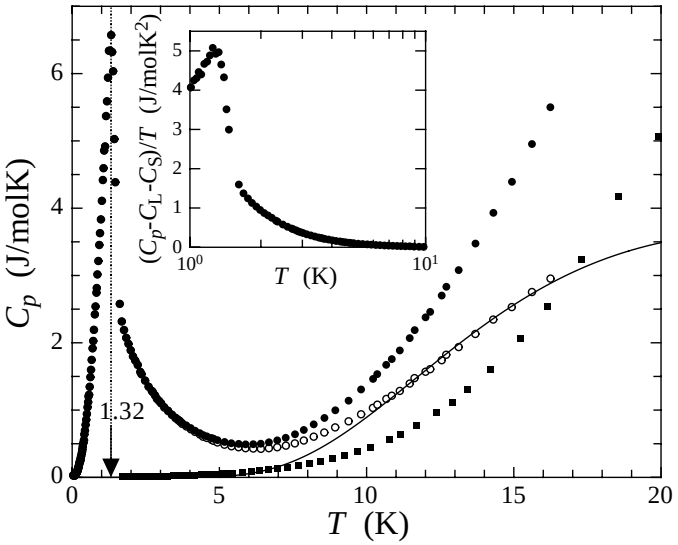

Fig. 1. Temperature dependence of the molar specific heat C_p of $CeAuAl_3$ (full circles) and of $LaAuAl_3$ (full squares). The λ–type anomaly has its maximum at 1.32 K. The open circles represent $C_p - C_L$ of $CeAuAl_3$, where C_L is the lattice contribution of $LaAuAl_3$. The solid curve is the fit according to equation (3). The inset shows $(C_p - C_L - C_S)/T$ *versus* $\log T$, where C_S is the contribution due to the Schottky anomaly.

3.1.1 Specific heat of $LaAuAl_3$

The specific heat of $LaAuAl_3$ is shown in Figure 1 as full squares. At low temperatures, $C_p(T)$ of $LaAuAl_3$ is well described by the common low–temperature electronic and lattice contributions, *i.e.*

$$C_p = \gamma T + \beta T^3, \tag{1}$$

as is shown in Figure 2. Fitting the data between 1.7 and 3.1 K (open circles in Fig. 2) to equation (1), we obtain $\gamma = 3.5$ mJ/molK^2 and $\beta = 0.24$ mJ/molK^4. The total lattice contribution C_L is determined by

$$C_L = C_p - \gamma T, \tag{2}$$

with the γ value given above. The resulting lattice contribution C_L of $LaAuAl_3$ is now subtracted from the total specific heat C_p of $CeAuAl_3$. The result, $C_p - C_L$, is shown as open circles in Figure 1.

3.1.2 Specific heat of $CeAuAl_3$ above T_N

It is obvious from Figure 1 that after the subtraction of C_L there remains a pronounced high–temperature contribution to the specific heat of $CeAuAl_3$. For symmetry reasons the sixfold degenerate $J = 5/2$ multiplets of the Ce^{3+}

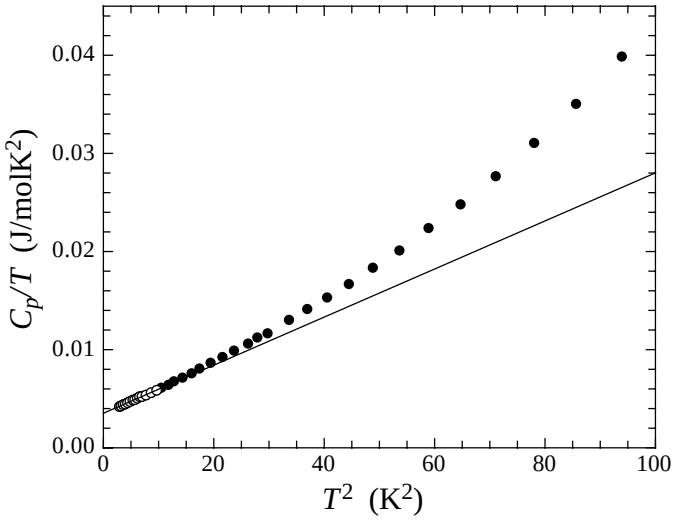

Fig. 2. Specific heat C_p of $LaAuAl_3$ plotted as C_p/T *versus* T^2. The solid straight line is the best fit to the data between 1.7 and 3.1 K (open circles) according to equation (1).

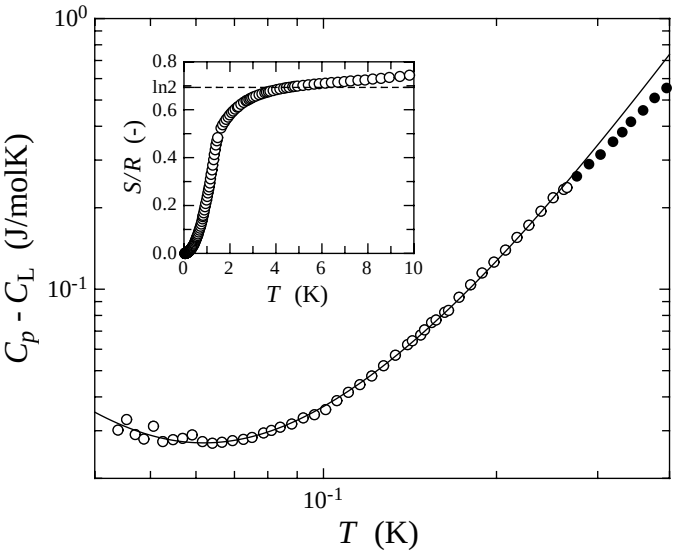

Fig. 3. Total specific heat C_p minus the lattice contribution C_L *versus* temperature T for $CeAuAl_3$ on a log–log plot. The curve is the best fit to the data shown as open circles using equation (6). The inset shows the entropy for electronic degrees of freedom per $CeAuAl_3$ formula unit, S/R, as a function of T.

ions are split into three doublet states. Therefore we assume that for $T < 20\,\mathrm{K}$ this excess specific heat may in a first approximation be described by a Schottky anomaly

$$C_\mathrm{S} = a_\mathrm{S}\frac{(\Delta/k_\mathrm{B}T)^2\exp{(\Delta/k_\mathrm{B}T)}}{(1+\exp{(\Delta/k_\mathrm{B}T)})^2}, \qquad (3)$$

resulting from excitations between two doublet states with an interlevel energy separation Δ. A fit of the data above 10 K, with a_S fixed to considering one doublet ground state and one doublet excited state per Ce atom, yields $\Delta/k_\mathrm{B} = 57\,\mathrm{K}$. The fit is shown as a solid curve in Figure 1.

As is shown in the inset of Figure 1, below 10 K $(C_\mathrm{p} - C_\mathrm{L} - C_\mathrm{S})/T$ increases gradually with decreasing T to 1.6 J/mol K^2 at 1.6 K, where a steeper increase sets in. While we attribute this steeper increase to the onset of the cooperative antiferromagnetic phase transition, the more gradual increase of $(C_\mathrm{p} - C_\mathrm{L} - C_\mathrm{S})/T$ from 10 to 1.6 K may, at least in part, be due to the onset of heavy–electron behaviour. However, a reliable determination of the itinerant–electron contribution γT to the specific heat in this temperature range is not possible because it cannot easily be distinguished from a likely contribution due to short range magnetic order fluctuations. An estimate of γ from our Hall effect data at temperatures well above T_N, to be presented below, yields $\gamma = 4.4\mathrm{mJ/molK}^2$, *i.e.*, there is virtually no enhancement above the value of $LaAuAl_3$.

3.1.3 Specific heat of $CeAuAl_3$ below T_N

Next we analyse the specific heat of $CeAuAl_3$ at temperatures below T_N. We consider three contributions to $C_\mathrm{p} - C_\mathrm{L}$: an electronic contribution $C_\mathrm{e} = \gamma T$, a nuclear hyperfine contribution C_N, and a magnetic contribution C_m. C_N is the specific heat due to excitations between hyperfine–split nuclear energy levels. Such a splitting may be induced either by the interaction of a nuclear–spin moment with an internal magnetic field or by the interaction of the nuclear quadrupole moment with an electric field gradient. At temperatures large compared to the energy splitting, the corresponding Schottky anomaly can be approximated by

$$C_\mathrm{N} = a_\mathrm{N}T^{-2}. \qquad (4)$$

As a magnetic contribution C_m we consider the specific heat due to spin–wave excitations which for a three–dimensional antiferromagnet with a linear spin–wave dispersion relation at $T < T_\mathrm{N}$ is predicted to be [12]

$$C_\mathrm{m} = a_\mathrm{m}T^3 = \frac{8\pi^2 R}{15}\left(\frac{T}{\Theta_\mathrm{c}}\right)^3, \qquad (5)$$

where Θ_c is a fit parameter of the order of the Néel temperature.

As is shown in Figure 3, the $C_\mathrm{p} - C_\mathrm{L}$ data of $CeAuAl_3$ can very well be described up to approximately $T_\mathrm{N}/5$ by

$$C_\mathrm{p} - C_\mathrm{L} = C_\mathrm{N} + C_\mathrm{e} + C_\mathrm{m} \qquad (6)$$

with $a_\mathrm{N} = 41\mu\mathrm{JK/mol}$, $\gamma = 227\,\mathrm{mJ/molK}^2$, and $a_\mathrm{m} = 10.1\,\mathrm{J/molK}^4$. The energy splitting corresponding to $a_\mathrm{N} = 41\mu\mathrm{JK/mol}$ is $k_\mathrm{B}T_\mathrm{n}$ with $T_\mathrm{n} = 4.4\,\mathrm{mK}$. Since T_n is one order of magnitude smaller than the lowest temperature reached in our C_p measurements, the approximation leading to equation (4) is appropriate here. The value obtained for a_m appears to be reasonable. From equation (5) we calculate $\Theta_\mathrm{c} = 1.63\,\mathrm{K}$, which is indeed of the order of T_N. The γ value determined below T_N is about 50 times higher

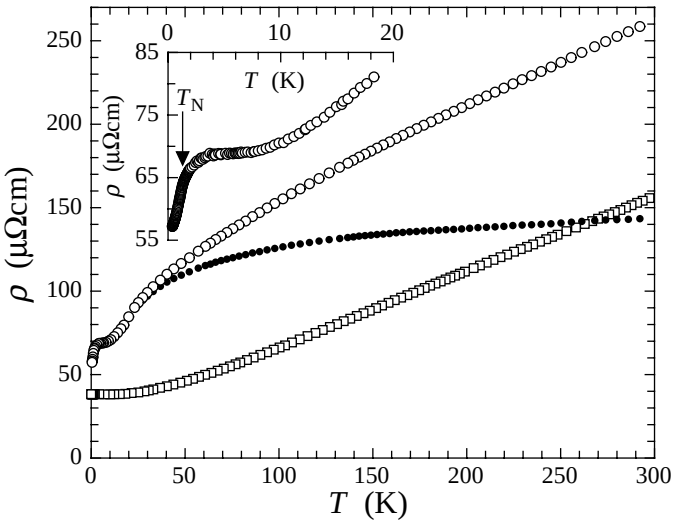

Fig. 4. Temperature dependence of the electrical resistivity $\rho(T)$ of $CeAuAl_3$ (open circles) and of $LaAuAl_3$ (open squares). The full circles represent $\rho - \rho_{ph}$ of $CeAuAl_3$, obtained as explained in the text. The inset shows $\rho(T)$ of $CeAuAl_3$ below 20 K.

than the one estimated from the high–temperature Hall effect data. This indicates that $CeAuAl_3$ turns into a highly correlated electronic system only at very low temperatures. The linear temperature dependence of the electronic specific heat with a γ value strongly enhanced over the free electron value is the Fermi–liquid behaviour typically observed in Kondo lattice systems at temperatures below the characteristic temperature T^*. As usually found experimentally, the fictitious Fermi temperature T_F^* associated with the molar Sommerfeld coefficient via $\gamma = \pi^2 R/(2T_F^*)$ is, with 180 K, considerably larger than the characteristic temperature T^*.

3.1.4 Entropy due to electronic degrees of freedom

In the inset of Figure 3 we show the entropy of $CeAuAl_3$ from electronic degrees of freedom calculated from

$$S(T) = \int_0^T \frac{C_p - C_L - C_N}{T} dT. \quad (7)$$

At approximately 4.5 K, the entropy per $CeAuAl_3$ formula unit, S/R, reaches $\ln 2$, indicating that the phase transition is due to a magnetic instability which involves the splitting of a doubly degenerate ground state. The temperature of 4.5 K, which is distinctly higher than the Néel temperature $T_N = 1.32$ K, may serve as an estimate of the Kondo lattice temperature T^*.

3.2 Electrical transport

In Figure 4 we present the temperature dependence of the electrical resistivity $\rho(T)$ of $CeAuAl_3$ and of $LaAuAl_3$ as open circles and open squares, respectively.

3.2.1 Electrical resistivity of $LaAuAl_3$

The resistivity of $LaAuAl_3$ decreases linearly with temperature from 300 to approximately 70 K. At lower temperatures, ρ tends to saturate to a constant value. The residual resistance ratio is $\rho(300\,K)/\rho(0\,K) = 4.1$. The simple temperature dependence of ρ suggests that the dominant scattering mechanisms in $LaAuAl_3$ are elastic impurity and defect scattering and electron–phonon scattering, resulting, with Matthiessen's rule, in

$$\rho(T) = \rho_{imp} + \rho_{ph}(T). \quad (8)$$

The impurity or defect contribution is $\rho_{imp} = 38.2\,\mu\Omega$cm. The phonon contribution varies approximately as $\rho_{ph} = c_1 T^5$ at $T < 20$ K, and as $\rho_{ph} = c_2 T$ at $T > 70$ K, as expected from the Bloch–Grüneisen description of $\rho_{ph}(T)$. The corresponding fits to the data yield $c_1 = 1.7 \times 10^{-7}\ \mu\Omega\text{cm/K}^5$ and $c_2 = 0.456 \times 10^{-7}\ \mu\Omega$cm/K. The ratio of the theoretical Bloch–Grüneisen expressions for $\rho(T_1)$ and $\rho(T_2)$ with $T_1 \ll \Theta < T_2$ results in [13] $\Theta_D^4 = 498 c_2/c_1$, from which we calculate the Debye temperature $\Theta_D = 190$ K. From the βT^3 term of the specific heat of $LaAuAl_3$ determined above we calculate a Debye temperature of 160 K, if the Debye approximation is applied only to the acoustic branches of the vibrational spectrum. Since this latter approximation gives a lower limit for the Debye temperature, the agreement between the Θ_D values estimated from both the resistivity and the specific heat data may be judged as satisfying.

3.2.2 Electrical resistivity of $CeAuAl_3$

The residual resistance ratio of $CeAuAl_3$ is $\rho(300\text{ K})/\rho(0\text{ K}) = 4.6$. From 300 K down to approximately 180 K, the temperature dependent term of $\rho(T)$ of $CeAuAl_3$ decreases roughly linearly. Towards lower temperatures, downward deviations from this linear behaviour set in. To better emphasize these deviations from linearity, we assume that the phonon contribution ρ_{ph} to the resistivity ρ of $CeAuAl_3$ is the same as ρ_{ph} of $LaAuAl_3$ and we plot $\rho - \rho_{ph}$ of $CeAuAl_3$ as full dots in Figure 4. Below 20 K, the phonon contribution to $\rho(T)$ is less than 1% and consequently the $\rho(T)$ and the $(\rho - \rho_{ph})(T)$ curves of $CeAuAl_3$ in Figure 4 merge. The remaining resistivity $(\rho - \rho_{ph})(T)$ decreases rather gradually from 300 K down to approximately 60 K, where a steeper decrease sets in. Together with the results of our magnetic susceptibility measurements, to be outlined below, we attribute the downward curvature of $(\rho - \rho_{ph})(T)$ with decreasing T to a reduced scattering when T is comparable to or less than the crystalline–electric–field–induced energy splitting of the Ce^{3+} $J = 5/2$ 4f electron levels.

Between 8 and 4 K, we observe a plateau in $\rho(T)$ with $\rho = 68.9\ \mu\Omega$cm, followed by a rather steep decrease of

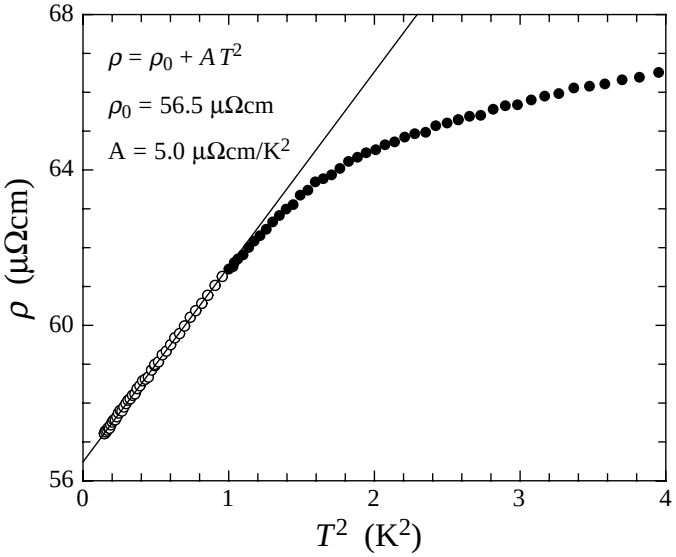

Fig. 5. Electrical resistivity ρ of $CeAuAl_3$ *versus* T^2 for $T < 2$ K. The open circles are the data points that were used for the fit according to equation (9), which is shown as a solid line.

$\rho(T)$ with T down to the lowest measured temperature of 0.38 K. Below 1 K, $\rho(T)$ is well approximated by

$$\rho(T) = \rho_0 + AT^2, \tag{9}$$

with $\rho_0 = 56.5\,\mu\Omega$cm and $A = 5.0\,\mu\Omega\text{cm/K}^2$ as is shown in Figure 5. The contributions ρ_0 and AT^2 of equation (9) are usually attributed to impurity scattering and to electron–electron scattering, respectively. The magnitude of the coefficient A is comparable to that of values found in heavy–electron compounds. It is unusual that a T^2 dependence persists up to $0.8T_\text{N}$. In particular, no magnetic contribution $\rho_\text{m} \propto T^3$, that may be expected when considering the spin–wave contribution to the specific heat $C_\text{m} \propto T^3$ discussed above, may be identified. In Kondo lattice systems the transition to Fermi–liquid behaviour with $\rho \propto T^2$ is expected at temperatures well below the Kondo lattice temperature T^* [1]. Since the T^2 dependence persists up to 1K for $CeAuAl_3$ we expect a Kondo lattice temperature of at least several Kelvin, in agreement with our estimate of $T^* \approx 4.5$ K from the temperature dependence of the electronic entropy.

The resistivity at the plateau between 4 and 8K may be attributed to the sum of a temperature independent magnetic resistivity ρ_m^0 and the residual defect contribution ρ_0. With $\rho_0 = 56.5\,\mu\Omega$cm from above, $\rho_\text{m}^0 = 12.4\,\mu\Omega$cm. The decrease of the magnetic resistivity $\rho_\text{m}(T)$ below 4 K reflects the reduction of spin fluctuations as the magnetic ordering sets in. However, the temperature at which ρ_m starts to drop is considerably higher than the Néel temperature $T_\text{N} = 1.32$ K. A possible second source for this drop of $\rho_\text{m}(T)$ is the onset of coherence in a Kondo lattice, which leads to a reduction of spin fluctuations by suppressing the magnetic moment on each Ce site.

3.2.3 Hall effect of $CeAuAl_3$

At all measured temperatures between 130 and 250 K, the Hall voltage V_H varied approximately linearly with the external magnetic field H and with the current I. The Hall coefficient, given by

$$R_\text{H} = \frac{V_\text{H} d}{I \mu_0 H} \tag{10}$$

with the sample thickness d and the permeability of free space μ_0, is approximately temperature independent with an average value $R_\text{H} = 7 \times 10^{-11}\ \text{C}/m^3$. The sign of R_H is positive indicating that the charge carriers are predominantly hole like. The Hall mobility $\mu_\text{H} = R_\text{H}/\rho$ at 200 K is, with 0.3 cm^2/Vs, quite low. We estimate the charge carrier concentration from $n = 1/(|R_\text{H} e|)$, where e is the electronic charge, to be $n = 9 \times 10^{22}\ \text{cm}^{-3}$, which corresponds to approximately 9 charge carriers per $CeAuAl_3$ formula unit. In a free electron approximation with an effective mass ratio $m/m_0 = 1$, this charge carrier concentration is compatible with an electronic specific heat coefficient $\gamma = 4.4\ \text{mJ/molK}^2$, as mentioned above.

3.3 Magnetic properties

3.3.1 Magnetic susceptibility of $LaAuAl_3$

As expected, the magnetic susceptibility of $LaAuAl_3$ is small compared to the magnetic susceptibility of $CeAuAl_3$ (smaller by three orders of magnitude at 2 K). It is thus justified to associate the magnetic properties of $CeAuAl_3$ solely with the presence of the Ce 4f electron. The small measured magnetic susceptibility of $LaAuAl_3$ is most probably extrinsic and might, for example, be due to some small amount of rare earth impurities in $LaAuAl_3$. Indeed, we may approximate $\chi(T)$ of $LaAuAl_3$ below 5 K by a Curie–Weiss law with $\Theta_\text{p} = -2$ K and an effective moment of $0.14\,\mu_\text{B}$ per formula unit. In the case of Ce^{3+} impurities, this corresponds to 2 ppm Ce^{3+} impurities per $LaAuAl_3$ formula unit.

3.3.2 High temperature magnetic susceptibility of $CeAuAl_3$

In Figure 6 we present the dc magnetic susceptibility of $CeAuAl_3$ in the form $1/\chi$ *versus* T. The two curves were obtained with two different sample orientations with respect to the direction of the magnetic field. Since the aspect ratio of the sample is close to one, the demagnetization factor is very similar for all sample orientations. For temperatures above 30 K we estimate the demagnetization field to be smaller than 0.5 % of the applied field. The lack of coincidence of the two curves in Figure 6 thus indicates that the crystallites in the bulk sample are not randomly oriented but have some preferential orientation.

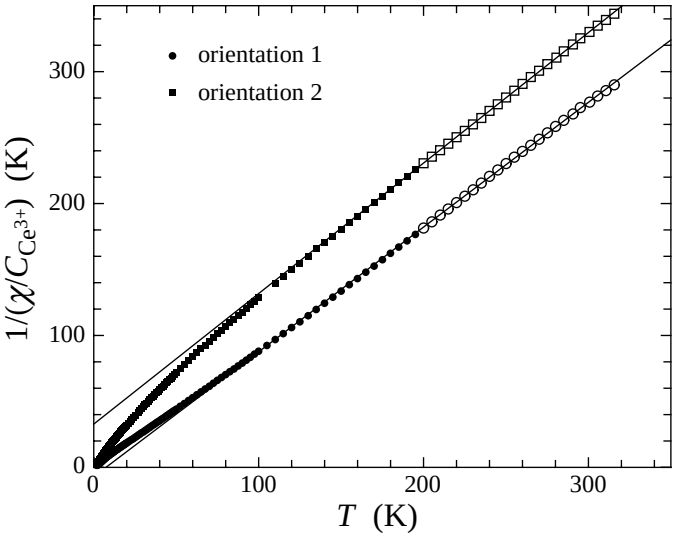

Fig. 6. Inverse dc magnetic susceptibility $1/\chi$ *versus* temperature T of $CeAuAl_3$. χ is taken per ion and normalized to the Curie constant of a free Ce^{3+} ion, $C_{Ce^{3+}} = p_{\rm eff}^2\mu_0/(3k_{\rm B})$ with $p_{\rm eff} = 2.54\mu_{\rm B}$. The two curves were obtained with two different orientations of the sample with respect to the direction of the magnetic field. The straight lines represent fits according to equation (11) to the data in the temperature range above 200 K (open symbols).

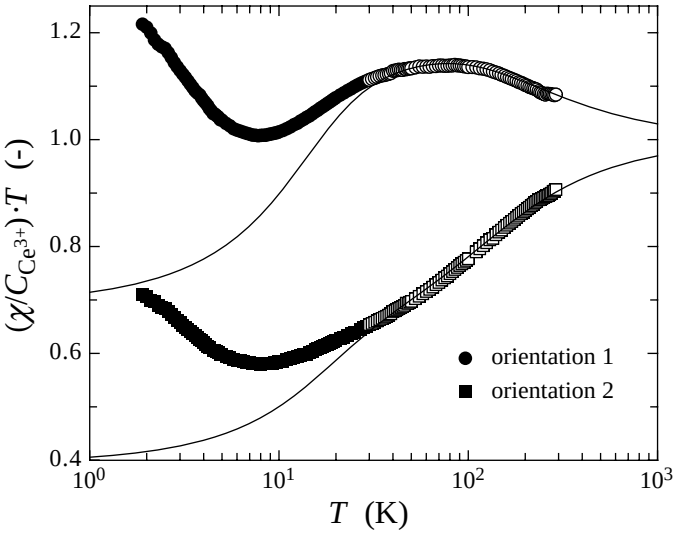

Fig. 7. Dc magnetic susceptibility χ multiplied by the temperature T as a function of $\log T$. χ is taken per ion and normalized to the Curie constant of a free Ce^{3+} ion, $C_{Ce^{3+}} = p_{\rm eff}^2\mu_0/(3k_{\rm B})$ with $p_{\rm eff} = 2.54\mu_{\rm B}$. The circles and the squares represent the data taken on the same specimen of $CeAuAl_3$, but with two different sample orientations with respect to the magnetic field **H**. The curves represent fits using the CEF model explained in the text to the data in the temperature range above 30 K (open symbols).

Since the structure of $CeAuAl_3$ is tetragonal, it is not surprising that a certain direction may be privileged during the synthesis of the material.

At $T > 200$ K, the data may be approximated by a Curie–Weiss law

$$\chi_{\rm per\ ion} = \frac{p_{\rm eff}^2\mu_0}{3k_{\rm B}(T-\Theta_{\rm p})} \tag{11}$$

with the effective moment $p_{\rm eff} = (J(J+1)g_J^2\mu_{\rm B}^2)^{1/2} = 2.61\mu_{\rm B}$ and the paramagnetic Curie temperature $\Theta_{\rm p} = 7.4$ K for orientation 1. For orientation 2, $p_{\rm eff} = 2.55\mu_{\rm B}$ and $\Theta_{\rm p} = -33$K. The $p_{\rm eff}$ values are close to $p_{\rm eff} = 2.54\mu_{\rm B}$ of a free Ce^{3+} ion, for which $J = 5/2$ and $g_J = 6/7$. In the following section we demonstrate that the $\chi(T)$ data in the temperature range $T > 30\,{\rm K} \approx 20\,T_{\rm N}$ may very well be described if the effect of the crystalline electric fields (CEF) on the six–fold degenerate $J = 5/2$ ground state multiplet of free Ce^{3+} is taken into account.

3.3.3 Crystalline electric field (CEF) effects

As mentioned above, the point–group symmetry of the Ce site in $CeAuAl_3$ is C_{4v}. According to point–group theory [14] the operator equivalent crystal–field Hamiltonian reduces to

$$\mathcal{H}_{\rm c} = B_2^0O_2^0 + B_4^0O_4^0 + B_4^4O_4^4 \tag{12}$$

where the O_l^m are operator equivalents and the B_l^m are proportional to the crystal field parameters A_l^m. Using the matrix elements $\left\langle 5/2, M'_{5/2}|O_l^m|5/2, M_{5/2}\right\rangle$ with $M_{5/2} = \pm 5/2$, $\pm 3/2$, and $\pm 1/2$, tabulated by Hutchings [15], and diagonalizing the energy matrix it is found that the $J = 5/2$ multiplet splits into three two–fold degenerate levels, one of which consists of the pure $|\pm 1/2\rangle$ states and the other two of which are linear combinations of the $|\pm 3/2\rangle$ and $|\pm 5/2\rangle$ states.

The magnetic susceptibility due to non–interacting moments, to second order in the magnetic field H, is given by [16]

$$\chi_{\rm per\ ion} = \frac{\mu_0\sum_n\left[\dfrac{(E_n^{(1)})^2}{k_{\rm B}T} - 2E_n^{(2)}\right]\exp\left(-E_n^{(0)}/k_{\rm B}T\right)}{\sum_n \exp\left(-E_n^{(0)}/k_{\rm B}T\right)} \tag{13}$$

where the $E_n^{(i)}$ are the energy corrections for the n–th level of i–th order in H. In general these corrections are different for **H** parallel and perpendicular to the **c**–axis of the crystal lattice, leading to $\chi_\parallel$ and $\chi_\perp$. The magnetic susceptibility of a polycrystalline sample may be written as

$$\chi = C_\parallel\chi_\parallel + (1-C_\parallel)\chi_\perp. \tag{14}$$

For randomly oriented crystallites, $C_\parallel = 1/3$.

In Figure 7 we replot the $\chi(T)$ data of Figure 6 in the form χT *versus* $\log T$. This presentation is most suitable for the study of CEF effects since it clearly reveals deviations from a Curie–Weiss type behaviour. A Curie–Weiss

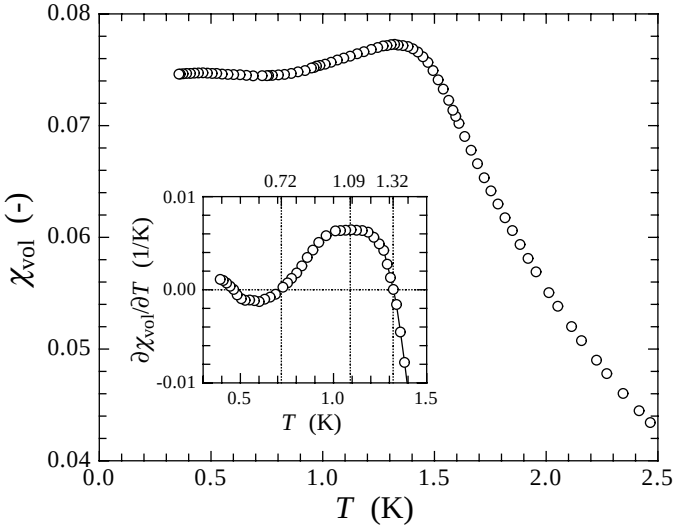

Fig. 8. Temperature dependence of the ac magnetic susceptibility $\chi(T)$ of $CeAuAl_3$ below 2.5 K. χ is the volume susceptibility expressed in SI units. The inset shows the numerical derivative $\partial\chi/\partial T$, calculated from the $\chi(T)$ data.

law with $\Theta_p = 0$ corresponds to a horizontal line in this plot, a positive value of Θ_p is reflected by a negative slope of $\chi T(T)$ and *vice versa*. The fit parameters are the energy separations $k_B T_I$ and $k_B T_{II}$ of the first and the second excited doublet from the ground state doublet, the ratio $\alpha = a_{\pm 3/2}/a_{\pm 5/2}$ of the coefficients of the $|\pm 3/2\rangle$ and $|\pm 5/2\rangle$ states in the linear combinations, and the coefficient $C_\parallel$ for each of the two sample orientations. A very good agreement between theory and experiment is obtained for the following set of parameters: $T_I = 57$ K, $T_{II} = 265$ K, $\alpha = 8.7$, $C_{\parallel 1} = 0.11$, and $C_{\parallel 2} = 0.55$, where $|\pm 1/2\rangle$ is the ground state doublet, $|\pm 3/2\rangle$ with a small admixture of $|\pm 5/2\rangle$ is the first excited doublet, and $|\pm 5/2\rangle$ with a small admixture of $|\pm 3/2\rangle$ is the second excited doublet. The parameter T_I was chosen as the temperature Δ/k_B characterizing the Schottky anomaly of the specific heat, determined in Section 3.1.2, the other parameters result from the fitting procedure.

The result of the fitting procedure of the data at $T > 30$ K is shown as the solid curves in Figure 7. The agreement is excellent for $T > 30$ K. The deviation of the data from the extrapolation of the fit to temperatures below 30 K is attributed to the growing importance of other interactions with decreasing temperature. The negative and positive slope of the curves at $T > 100$ K reflect a positive and a negative value for Θ_p in our Curie–Weiss fits of Section 3.3.2, respectively. At the highest measured temperatures the $\chi T(T)$ data, which have been normalized to the Curie constant of free Ce^{3+} ions, tend to converge to the value one, *i.e.*, the expected behaviour of an ensemble of free Ce^{3+} ions is indeed approached at elevated temperatures.

3.3.4 Magnetic susceptibility of $CeAuAl_3$ close to T_N

In Figure 8 we show the ac magnetic susceptibility χ of $CeAuAl_3$ as a function of temperature below 2.5 K. $\chi(T)$ has a maximum at 1.32 K, an inflection point at 1.09 K, and a very shallow minimum at 0.72 K, as is emphasized by the inset of Figure 8, showing the derivative $\partial\chi/\partial T$ *versus* T. The temperature of the maximum of $\chi(T)$ coincides with the temperature of the maximum of the specific heat anomaly shown in Figure 1 and thus supports the phenomenological choice of the Néel temperature T_N.

The Pauli susceptibility that one may associate with the γ value of 227 mJ/molK^2 derived from the low–temperature specific heat data is, with 6.4×10^{-4}, small compared to the magnetic susceptibility observed below T_N.

4 Conclusions

This comprehensive study of thermodynamic and electrical transport properties of $CeAuAl_3$ allows to classify this compound as a heavy–electron antiferromagnet.

The analysis of the data is made easier and more reliable because of the simple metallic behaviour of the non–magnetic reference compound $LaAuAl_3$. The features of the specific heat C_p, the magnetic susceptibility χ, and the electrical resistivity ρ of $CeAuAl_3$ may thus unambiguously be associated with the presence of the 4f electron of Ce.

The temperature variation of the magnetic susceptibility at high temperatures is interpreted in terms of crystalline electric field (CEF) effects. The energy separations of the first and second excited doublet with respect to the ground state doublet derived in our analysis are $k_B T_I$ and $k_B T_{II}$, with $T_I = 57$ K and $T_{II} = 265$ K. Thermal excitations to the first excited doublet are manifest in a low–temperature tail of a Schottky anomaly of the specific heat. The falloff of $\rho(T)$ below T_I and the more gradual decrease of $\rho(T)$ below T_{II} reflect the reduction of scattering from a magnetic doublet with decreasing T and are, as such, evidence for a non–negligible interaction of the conduction electrons with the localized 4f electrons.

The distinct anomalies in $C_p(T)$ and $\chi(T)$ indicate that $CeAuAl_3$ orders antiferromagnetically at the Néel temperature $T_N = 1.32$ K. The molar entropy release by the phase transition of $R \ln 2$ is in agreement with the double degeneracy of the CEF–split ground state being lifted by a magnetic instability. The fact that $R \ln 2$ is reached only at approximately $3.5 T_N$ suggests that the Kondo interaction operates in parallel with the RKKY interaction and provides an estimate of the Kondo lattice temperature T^* of approximately 4.5 K.

At the lowest temperatures (below 1 K) the typical hallmarks of a Fermi liquid are observed, *i.e.*, a quadratic

temperature dependence of the resistivity and a linear–in–T contribution to the specific heat. The large electronic specific heat coefficient $\gamma = 227\,\mathrm{mJ/molK^2}$, which is more than 50 times higher than its value determined at temperatures well above T_N, and the large coefficient $A = 5\,\mu\Omega\mathrm{cm/K^2}$ of the quadratic–in–T term of the electrical resistivity indicate that correlated electrons with enhanced effective masses develop in parallel to the onset of magnetic order. As argued by Mentink *et al.* [7], enhanced γ values might also result from a Schottky anomaly arising from a very small energy separation of the first excited CEF doublet with respect to the ground state doublet, combined with a site–disorder–induced broadening of the antiferromagnetic transition. For $CeAuAl_3$ we can, with some confidence, exclude this origin of an enhanced γ value since the Schottky anomaly due to the splitting $k_\mathrm{B}T_\mathrm{I}$ with $T_\mathrm{I} = 57\,\mathrm{K}$ has a negligible influence at $T < 1\,\mathrm{K}$. Also site–disorder is expected to be small in $CeAuAl_3$ which crystallizes, unlike $CeTMAl_3$ with TM = Pd, Pt, Cu, in the atomically *ordered* $BaNiSn_3$–type structure. We thus argue that $CeAuAl_3$ shows genuine heavy–electron behaviour at very low temperatures. The small magnitude of T_N and the similar magnitude of T_N and T^* indicate that $CeAuAl_3$ is close to the quantum critical point, which might be reached by varying external parameters like, *e.g.*, pressure.

Thus $CeAuAl_3$ seems, like $CePd_2In$, to be another well suited model compound for a more detailed study of the interplay of strong electronic correlations and RKKY–induced antiferromagnetism. In particular, neutron diffraction or other microscopic studies would quite likely reveal more details of the nature of the antiferromagnetic state in $CeAuAl_3$. For $CePd_2In$ it has been shown [3] by nuclear magnetic resonance experiments that the magnitude of the Ce moments is considerably reduced in the magnetically ordered state, indicating a sizable Kondo screening.

We thank S. Sigrist for the sample synthesis and H. Thomas for technical assistance. We are grateful to M. A. Chernikov for his help during part of the measurements. Part of this work was financially supported by the Schweizerischer Nationalfonds zur Förderung der Wissenschaftlichen Forschung.

References

1. see, *e.g.*, N. Grewe and F. Steglich, in *Handbook on the Physics and Chemistry of the Rare Earths*, edited by K. A. Gschneidner and L. Eyring (North Holland, Amsterdam, 1991), Vol. 14, p. 343 ff.
2. H.R. Ott, J. K. Kjems, F. Hulliger, Phys. Rev. Lett. **42**, 1378 (1979).
3. J.L. Gavilano, P. Vonlanthen, B. Ambrosini, J. Hunziker, F. Hulliger, H.R. Ott, Europhys. Lett. **32**, 361 (1995).
4. F. Hulliger, J. Alloys Comp. **218**, 255 (1995).
5. C. Schank, F. Jährling, L. Luo, A. Grauel, C. Wassilew, R. Borth, G. Olesch, C.D. Bredl, C. Geibel, F. Steglich, J. Alloys Comp. **207/208**, 329 (1994).
6. M. Kontani, H. Ido, H. Ando, T. Nishioka, Y. Yamaguchi, J. Phys. Soc. Jpn **63**, 1652 (1994).
7. S.A.M. Mentink, N.M. Bos, B.J. van Rossum, G.J. Nieuwenhuys, J.A. Mydosh, K.H.J. Buschow, J. Appl. Phys. **73**, 6625 (1993).
8. Y.N. Grin, P. Rogl, K. Hiebl, F.E. Wagner, H. Noël, J. Solid State Chem. **70**, 168 (1987).
9. L. Menon, S.K. Dhar, S.K. Malik, Physica B **223/224**, 283 (1996).
10. F. Hulliger, J. Alloys Comp. **200**, 75 (1993).
11. H. Schwer, private communication.
12. see, *e.g.*, S.V. Vonsovskii, *Magnetism* (John Wiley and Sons, New York, 1974), Vol. 2, p. 876.
13. see, *e.g.*, W. Brauer, *Einführung in die Elektronentheorie der Metalle* (Akademische Verlagsgesellschaft, Leipzig, 1972), p. 172 ff.
14. S.L. Altmann, P. Herzig, *Point–group theory tables* (Clarendon Press, Oxford, 1994).
15. M.T. Hutchings, in *Solid state physics*, edited by F. Seitz, D. Turnbull (Academic Press, New York, 1964), Vol. 16, p. 227 ff.
16. see, *e.g.*, R.M. White, *Quantum Theory of Magnetism*, Vol. 32 of Springer series in solid-state sciences (Springer–Verlag, Berlin, 1983), p. 14.